Organometallic derivatives of cyclotriphosphazene as precursors of nanostructured metallic materials: A new solid state method

Carlos Díaz*[†], María Luisa Valenzuela[†], Luis Zúñiga[†] and Colm O'Dwyer [‡]

[†]Departamento de Química, Facultad de Ciencias, Universidad de Chile, Las Palmeras 3425, Santiago, Chile. E-mail: cdiaz@uchile.cl
[‡]Department of Physics, and Materials & Surface Science Institute, University of Limerick, Limerick, Ireland.

Abstract The cyclic phosphazene trimers $[N_3P_3(OC_6H_5)_5\,OC_5H_4N{\cdot}Ti(Cp)_2Cl][PF_6]$ (**3**), $[N_3P_3(OC_6H_4CH_2CN{\cdot}Ti(Cp)_2Cl)_6]\,[PF_6]_6$ (**4**), $[N_3P_3(OC_6H_4\text{-}Bu^t)_5(OC_6H_4CH_2CN{\cdot}Ti(Cp)_2Cl)][PF_6]$ (**5**), $[N_3P_3(OC_6H_5)_5C_6H_4CH_2CN{\cdot}Ru(Cp)(PPh_3)_2][PF_6]$ (**6**), $[N_3P_3(OC_6H_5)_5C_6H_4CH_2CN{\cdot}Fe(Cp)(dppe)][PF_6]$ (**7**) and $N_3P_3(OC_6H_5)_5OC_5H_4N{\cdot}W(CO)_5$ (**8**) were prepared and characterized. As a model, the simple compounds $[HOC_5H_5N{\cdot}Ti(Cp)_2Cl]PF_6$ (**1**) and $[HOC_6H_4CH_2CN{\cdot}Ti(Cp)_2Cl]\,PF_6$ (**2**) were also prepared and characterized. Pyrolysis of the organometallic cyclic trimers in air yields metallic nanostructured materials, which according to transmission and scanning electron microscopy (TEM/SEM), energy-dispersive X- ray microanalysis (EDX), and IR data, can be formulated as either a metal oxide, metal pyrophosphate or a mixture in some cases, depending on the nature and quantity of the metal, characteristics of the organic spacer and the auxiliary substituent attached to the phosphorus cycle. Atomic force microscopy (AFM) data indicate the formation of small island and striate nanostructures. A plausible formation mechanism which involves the formation of a cyclomatrix is proposed, and the pyrolysis of the organometallic cyclic phosphazene polymer as a new and general method for obtaining metallic nanostructured materials is discussed.

1 Introduction

The development of manometer-sized materials is of profound interest from both theoretical and practical viewpoints, since they exhibit unique properties that are observed in neither individual molecules nor in bulk materials [1-6]. Chemical techniques are widely used to produce nanostructured materials due to their straightforward nature and the potential for producing large quantities of the final product. A crucial aspect is the stabilization of the metallic nanoparticles. The majority of these methods are carried out in solution, and stabilization can be electrostatic or steric [4]. Steric stabilization can be achieved by ligands, polymers, oligomers or solvents. However, few solid state methods for preparing metallic nanoparticles have been reported [7-11] and almost all of them involve gold nanoparticles [8, 9].

Polyphosphazene polymers $[N=PR_2]_n$ can bind metal ions and organometallic fragments through the R containing a donor group [12-18] (or with basic nitrogen in some cases). This suggests the possibility of stabilizing metal nanoparticles. In fact, Allcock et al. [19] reported the preparation in water of CdS nanoparticles entrapped in a polyphosphazene network MEEP (MEEP=poly(bis(2-(2'-methoxyethoxy)ethoxy)phosphazene). Wisian–Neilson [20] prepared gold nanoparticles in PMPP by reducing $AuCl_4$ with $NaBH_4$ in the presence of PMPP (PPMP= poly(methylphenylphosphazene) using a biphasic water/toluene system. Recently Wisian–Neilson [21] prepared Au nanoparticles using the method of Brust-Schiffrin in water/toluene, stabilizing the nanoparticles with thioether groups anchored to a polyphosphazene backbone (all of these methods are in solution). We have recently reported the first solid–phase synthesis of metal nanoparticles using polyphosphazene as a hybrid inorganic-organic template [22-25], shown in Scheme 1.

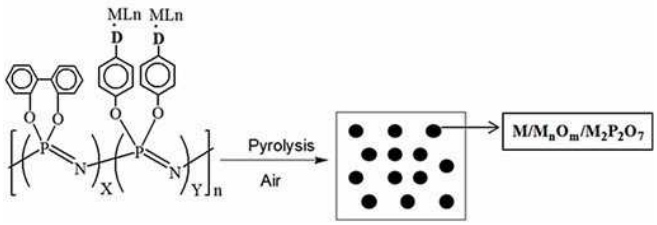

Scheme 1. Nanostructured metallic product from the pyrolysis of polyphosphazene with anchored organometallic fragments.

The method consists of the solid-state pyrolysis of the organometallic polyphosphazene precursor in air at 800°C. The inorganic polymer acts as a template permitting a uniform distribution of the metal centers through the chain, which after burning, looses the organic material as CO_2, and the phosphorus forms pyrophosphate and phosphorus oxides which are precursors of the final products, and/or form the stabilizer matrix. Although this method is a versatile route to metallic nanostructured oxides and pyrophosphates, some disadvantages are also evident, namely the tedious preparation procedures of the precursors. This disadvantage could be overcome by using the organometallic derivatives of cyclotriphosphazenes as precursors. The aim of this work was to investigate this possibility.

In this paper we report for the first time the formation of nanostructured transition metallic nanoparticles from the solid state pyrolysis of organometallic derivatives of a cyclotriphosphazene. We have reported recently the synthesis, characterization and pyrolysis studies of the silicon derivatives $N_3P_3[NH(CH_2)_3Si(OEt)_3]_6$, $N_3P_3[NH(CH_2)_3Si(OEt)_3]_3[NCH_3(CH_2)_3CN]_3$ and $N_3P_3[NH(CH_2)_3Si(OEt)_3]_3[OC_6H_4(CH_2)CN]_3$ [26]. The precursors studied in this work are shown in Scheme 2. We have previously reported several organometallic derivatives of cyclic phosphazenes [27-31] and here report the pyrolysis studies of such compounds. We also report for the first time the organometallic derivatives of Ti (**3**)-(**5**) as precursors. Although a considerable number of cyclotriphosphazenes are known [27-36] those of Ti [36] are relatively scarce.

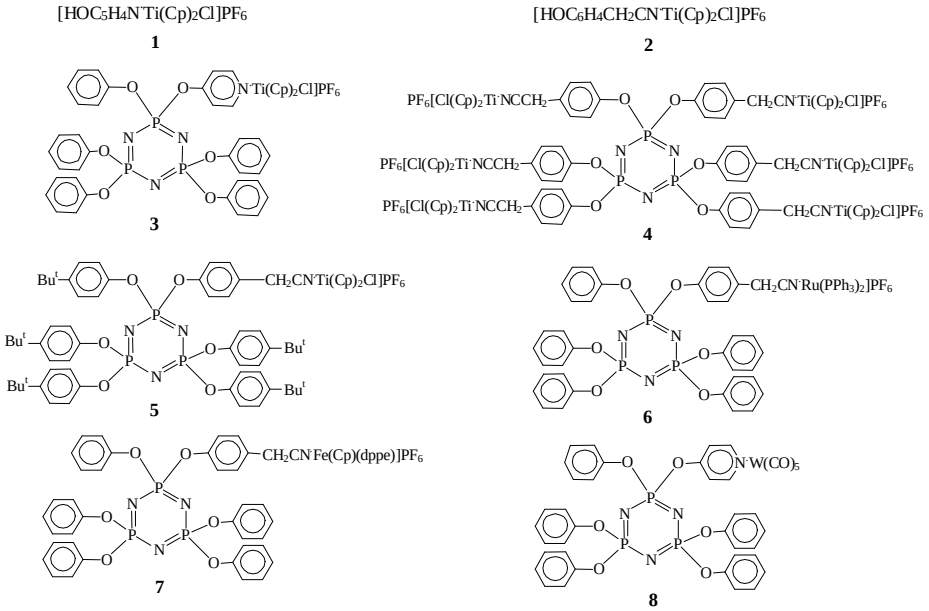

Scheme 2. Schematic representation of the formulae for the organometallic derivatives of phosphazene trimer precursors

2 Experimental Part

2.1 Physico-Chemical Measurements

All reactions were carried out under dinitrogen using standard Schlenk techniques. IR spectra were recorded on an FT-IR Perkin-Elmer 2000 spectrophotometer. Solvents were dried and purified using standard procedures. HOC_5H_5N, $HOC_6H_4CH_2CN$, $Ti(Cp)_2Cl_2$ and NH_4PF_6 were purchased from Sigma-Aldrich. NMR spectra were recorded on a Bruker AC-300 instrument using $CDCl_3$ as solvent unless otherwise stated. ^1H and $^{13}C\{^1H\}$ NMR are given in δ relative to TMS. $^{31}P\ \{^1H\}$ are given in δ relative to external 85% aqueous H_3PO_4. Coupling constants are in Hz. Thermogravimetric analysis (TGA) and differential scanning calorimetry (DSC) measurements were performed on a Mettler TA 4000 instrument and Mettler DSC 300 differential scanning calorimeter, respectively. The polymer samples were heated at a rate of 10 ºC/min from ambient temperature to 1000ºC under a constant flow of nitrogen.

2.2 Electron Microscopy

SEM photographs were taken with a Philips EM 300 microscope. EDAX (energy dispersive X-ray analysis) microanalysis was performed on a NORAN Instrument micro-probe attached to a JEOL 5410 scanning electron microscope. TEM analysis was conducted on a JEOLSX100 transmission microscope. The finely powered samples were dispersed in *n*-hexane and dropped on a conventional holey carbon copper grid and dried under a lamp.

2.3 Pyrolysis Experiments

The pyrolysis experiments were conducted by pouring a weighed portion (0.05–0.15 g) of the organometallic trimer into aluminum oxide boats that were placed in a tubular furnace (Lindberg/Blue Oven model STF55346C-1) under a flow of air, heating from 25 to 300°C and then to 800°C, and annealing for 2 h. The heating rate was 10°C/min under an air flow of 200 mL/min. The ligands $N_3P_3(OC_6H_5)_5OC_5H_4N$ [22], $N_3P_3(OC_6H_4CH_2CN)_6$ [31] and $N_3P_3(OC_6H_5)_5OC_6H_4CH_2CN$ [31], $N_3P_3(OC_6H_4\text{-}Bu^t)_5OC_6H_4CH_2CN$ [27] and the precursors $[N_3P_3(OC_6H_5)_5OC_6H_4CH_2\ CN{\cdot}Ru(Cp)(PPh_3)_2][PF_6]$ [28] (**6**), $[N_3P_3(OC_6H_5)_5OC_6H_4CH_2\ CN{\cdot}Fe(Cp)(dppe)][PF_6]$

[28] (**7**), and $N_3P_3(OC_6H_5)_5OC_5H_4N{\cdot}W(CO)_5$ [22] (**8**) were prepared as reported previously.

2.4 Preparation of $[HOC_5H_5N{\cdot}Ti(Cp)_2Cl]PF_6$ (**1**)

A mixture of HO-C_5H_4N (0.072 g, 0.8 mmol), and Cp_2TiCl_2 (019 g, 0.8 mmol) in the presence of NH_4PF_6 (0.196 g, 1.2 mmol) in methanol (70 mL), was stirred for 45 min at room temperature. The solvent was removed under reduced pressure and the red-oil residue extracted with CH_2Cl_2, filtered through Celite, and concentrated to ca. 10 mL. A 1:1 n-hexane/diethyl ether mixture was added and the red-orange powered precipitate was washed twice with the same solvent mixture and dried under reduced pressure. Yield: 0.25 g (49%). IR (KBr pellet, cm^{-1}) 3327m, 3105s, 2958m, 2930m, 2873m, 1728m, 1638s, 1513m, 1441w, 1360m, 1286m, 1192w, 1121w, 1075w, 1041w, 1017w, 834vs, 702w, 558m. ^{1}H-NMR ($CDCl_3$): 8.84, 8.82 (*o*-H, OC_5H_4N), 7.1-6.91 (m, OC_6H_5), 7.55, 7.53 (*m*-H, OC_5H_4N), 6.75 (C_5H_5), ^{13}C NMR{^{1}H} ($CDCl_3$, ppm): 142.97, 120.038, 114.41 (OC_5H_4N), 120.8 (C_5H_5). Anal. Calcd. for $C_{15}H_{16}NF_6OPClTi$: C 42,88, H 3.81, N 3.33; found C 42.1, H 3.57, N 3.29

2.5 Preparation of $[HOC_6H_4CH_2CN{\cdot}Ti(Cp)_2Cl]PF_6$ (**2**)

A mixture of HO-$C_6H_4CH_2CN$ (0.21 g, 1.58 mmol) and Cp_2TiCl_2 (0.464g, 1.86 mmol) in the presence of NH_4PF_6 (0.34 g, 2.11 mmol) in methanol (70 mL) was stirred for 24 h at room temperature. The solvent was removed under reduced pressure and the red-oil residue extracted with CH_2Cl_2, filtered through Celite and concentrated to ca. 10 mL. A 1:1 n-hexane/diethyl ether mixture was added and the red-orange powered precipitate was washed twice with the same solvent mixture and dried under reduced pressure. Yield: 0.25 g (49%). IR (KBr pellet, cm^{-1}) 3384m, 3113s, 2960w, 2857w, 1616w, 1516m, 1445m, 1266.2m, 1245m, 1145w, 1048s, 830vs, 702w, 558s. ^{1}H-NMR ($CDCl_3$): 7.20, 7.20 (*o*-H, OC_5H_4N), 6.87-6.81 (*m*-H, OC_5H_4N) 6.81 (C_5H_5), 6.66, 6.5 6.47 (OC_6H_4), 3.73, 3.75 (CH_2). ^{13}C NMR{^{1}H} ($CDCl_3$, ppm): 158.48, 130.786, 117.04 (OC_5H_4N), 130.786, 123.41, 121.851, 120.159(C_6H_4), 120.92 (C_5H_5), 116.36 (CN) , 23.23 (CH_2). Anal. Calcd. for $C_{18}H_{17}NF_6OPClTi$: C 46.83, H 3.69, N 3.03; found: C 45.1, H 3.9, N 2.99.

2.6 Preparation of $[N_3P_3(OC_6H_5)_5OC_5H_4N{\cdot}Ti(Cp)_2Cl]PF_6$ (**3**)

A mixture of $N_3P_3(O\text{-}C_6H_5)_5(OC_5H_4N)$ (0.58g, 0.83 mmol) and $Ti(Cp)_2Cl_2$ (0.211g, 0.84 mmol) in the presence of NH_4PF_6 (0.207 g, 1.27 mmol) in methanol (70 mL) was stirred for 3 h at room temperature. The solvent was removed under reduced pressure and the residue extracted with CH_2Cl_2, filtered through Celite and concentrated to ca. 10 mL. A 4:1 n-hexane/diethyl ether mixture was added and the yellow powdered precipitate was washed twice with the same solvent mixture and dried under reduced pressure. Yield: 0.75 g (75%). IR (KBr pellet, cm^{-1}) 3104w, 2967m, 2878w, 1635m, 1591m, 1488s, 1269m, 1243m, 1193s, 1178s, 1161s, 1070s, 1024w, 953vs, 881w, 839vs, 772m, 689m. ^{1}H-NMR ($CDCl_3$): 8.57, 8.50 (*o*-H, OC_5H_4N), 7.04, 7.02 (*m*-H, OC_5H_4N) 6.96 (C_5H_5), 6.94, 7.35 (OC_6H_4). ^{13}C NMR{^{1}H} ($CDCl_3$, ppm): 129.69, 120.29. 120.197 (OC_5H_4N), 120.9 (C_5H_5). ^{31}P NMR{^{1}H} (acetone-d_6) 8.82 (N_3P_3, ring), -144.12 (PF_6). Anal. Calcd. for $C_{48}H_{39}N_4F_6O_6P_4ClTi$: C 54.38, H 3.69, N 5.28; found: C 53.90, H 3.27, N 5.10.

2.7 Preparation of $[N_3P_3(OC_6H_4CH_2CN{\cdot}Ti(Cp)_2Cl)_6][PF_6]_6$ (**4**)

A mixture of $N_3P_3(OC_6H_4CH_2CN)_6$ (1.0 g, 1.07 mmol), and Cp_2TiCl_2 (1.40 g, 5.62 mmol) in the presence of NH_4PF_6 (1.61 g, 9.87 mmol) in methanol (90 mL) was stirred for 3h at room temperature. The solvent was removed under reduced pressure and the red-oil residue extracted with CH_2Cl_2, filtered through Celite and concentrated to ca. 10 mL. A 1:1 n-hexane/diethyl ether mixture was added and the red-orange powered precipitate was washed twice with the same solvent mixture and dried under reduced pressure. Yield: 2.1 g (52%). IR (KBr pellet, cm^{-1}) 3105m, 2967m, 2880w, 2252vw, 1604w, 1507m, 1474m, 1441m, 1270m, 1261m, 1165m, 1017m, 958m, 837vs, 739w, 557s. ^{1}H-NMR ($CDCl_3$) 6.66 (C_5H_5), 6.82, 6.72, 6.55, (OC_6H_4), 3.46, 3.42 (CH_2). ^{31}P NMR{^{1}H} (acetone-d_6) 9.15 (N_3P_3,ring), -144.12(PF_6). Anal. Calcd. for $C_{120}H_{96}N_9F_{36}O_6P_9Cl_6Ti_6$: C 44.70, H 2.98, N 3.91; found: C 44.89, H 2.88, N 3.79.

2.8 Preparation of $[N_3P_3(OC_6H_4\text{-}Bu^t)_5(OC_6H_4CH_2CN{\cdot}Ti(Cp)_2Cl)][PF_6]_6$ (**5**)

A mixture of $N_3P_3(OC_6H_4\text{-}Bu^t)_5(OC_6H_4CH_2CN)$ (1.52 g, 1.49 mmol), and Cp_2TiCl_2 (0.37 g, 1.48 mmol) in the presence of NH_4PF_6 (0.31 g, 1.87 mmol) in methanol (50 mL) was stirred for 3h at room temperature. The solvent was removed under reduced pressure and the red-oil residue extracted with CH_2Cl_2 (50 mL), filtered through Celite and concentrated to ca. 10 mL. A 1:1 n-hexane/diethyl ether mixture was added and the red-orange powered precipitate was washed twice with the same solvent mixture and dried under reduced pressure. Yield: 1.5 g (67%). IR (KBr pellet, cm^{-1}) 3105m, 2967m, 2880w, 2252vw, 1604w, 1507m, 1474m, 1441m, 1270m, 1261m, 1165m, 1017m, 958m, 837vs, 739w, 557s. ^{1}H-NMR ($CDCl_3$) 6.74-6.67 OC_6H_4, 6.66 (C_5H_5), 3.46, 3.48, (CH_2) 0.99 $C(CH_3)_3$. ^{13}C NMR{^{1}H} 125.77, 120, 114.82 (OC_6H_4) 120.9 (C_5H_5) 120.3 (CN), 28.9 $C(CH_3)_3$, 23.62 (CH_2). ^{31}P NMR{^{1}H} (acetone-d_6) 9.1 (N_3P_3,ring), -144.11(PF_6). Anal. Calcd for $C_{68}H_{86}N_4F_6O_6P_4ClTi$: C 60.20, H 5.80, N 4.01; found: C 58.73, H 5.98, N 3.97.

3 Results and Discussion

3.1 Preparation of Organometallic Precursors

According to Allcock's approximation [37], the simple model complexes (**1**) and (**2**) of the most complex cyclotriphosphazene titanium cyclopentadienyl derivatives have been also prepared. The models (**1**) and (**2**) were synthesized by reaction of the respective phenols, HO-C_5H_4N and HO-$C_6H_4CH_2CN$ with Cp_2TiCl_2 in the presence of NH_4PF_6 and in methanol as solvent. Complexes (**1**) and (**2**) were obtained as orange solids and characterized by elemental analysis, IR and ^{1}H, ^{31}P and ^{13}C NMR spectroscopy. Coordination of both phenols was also confirmed by the appearance of a strong band at 834 cm^{-1} for (**1**) and at 830 cm^{-1} for (**2**)**,** assigned to $\nu(PF_6)$, as well as by the ^{31}P-NMR signal of the PF_6 group at -144 ppm. In the case of complex (**1**), coordination of the organometallic fragment was evident by the typical shift of the *o*-H signal of the pyridine group, which changed from 7.98 ppm in free HO-C_5H_4N to 8.84 and 8.82 ppm upon coordination [22]. On the other hand, as found for nitriles, coordination causes a decrease of the intensity of the ν(CN) band [27, 28]. Other typical IR bands as well as ^{1}H- and ^{31}P-NMR signals were also observed, see the Experimental section. The ^{13}C-NMR signal of the C_5H_5 group of Cp_2Ti was observed at 120.03 ppm and 120.92 ppm, respectively, for (**1**) and (**2**); slightly shifted due to coordination effects.

3.2 $[N_3P_3(OC_6H_5)_5OC_5H_4N{\cdot}Ti(Cp)_2Cl]PF_6$ (**3**)

Reaction of $N_3P_3(OC_6H_5)_5OC_5H_4N$ with Cp_2TiCl_2 in the presence of NH_4PF_6 yielded $[N_3P_3(OC_6H_5)_5OC_5H_4N{\cdot}Ti(Cp)_2Cl]PF_6$, as an orange solid. Bonding of the organometallic fragment to the pyridine-ligand was evident from the absence of the strong ν(CC) oxypyridine band at 1589 cm^{-1} and the appearance of a new band at 1592cm^{-1} typical of oxypyridine coordination [18, 29]. Thus the expected ν(PF_6) band was observed normally at -144.12 ppm. Of special significance in the NMR spectrum was the effect of pyridinoxy groups on the *o*-H signals, which increase from 8.38 and 8.37 in $N_3P_3(OC_6H_5)_5\,OC_5H_4N$ to 8.50 and 8.57 ppm in (**3**) upon coordination. Thus, in the ^{13}C-NMR spectrum, the signal observed at 120.9 ppm was assigned to the C_5H_5 group of $Ti(Cp)_2Cl$ coordinated with the oxypyridine nitrogen on the basis of the respective value found for the model (**1**) 120.8 ppm. Similarly, in the ^{1}H NMR spectrum the signal of this group was seen at 6.96 ppm, in agreement with those observed for model (**1**), i.e. 6.75 ppm. Other ^{1}H and ^{13}C signals were also found (see Experimental section). In addition, the ^{31}P-NMR signal was seen at 8.82 ppm, slightly shifted with respect to the free ligand [27-31] 8.46 ppm, due to coordination effects.

3.3 $[N_3P_3(OC_6H_4CH_2CN{\cdot}Ti(Cp)_2Cl)_6][PF_6]_6$ (**4**)

Reaction of $N_3P_3(OC_6H_4CH_2CN)_6$ with Cp_2TiCl_2 yielded $[N_3P_3(OC_6H_4CH_2CN{\cdot}Ti(Cp)_2Cl)_6][PF_6]_6$ as an orange solid. Coordination of the organometallic fragment with the cyanide-ligand was evident from the increase in the frequency of the ν(CN) band from 2247 cm^{-1} in the free ligand to 2252 cm^{-1}, a behavior typical of the coordination of nitriles with organometallic complexes [27-31]. Thus the expected ν(PF_6) band was found normally at -144.12 ppm.

In the ^{31}P-NMR spectrum the signal at 9.15 ppm was shifted with respect to that of the free ligand, to 11.89 ppm, clearly indicating the coordination of the ligand. The ^{1}H-NMR spectrum shows a signal at 6.66 ppm assigned to the proton of the C_5H_5 group of $Ti(Cp)_2Cl$ coordinated to nitrile, which compares well with those of 6.81 ppm found for the Cp_2TiCl moiety in model (**2**). Other ^{1}H and ^{13}C signals were also observed (see Experimental section) in agreement with those of the respective model (**2**).

3.4 $[N_3P_3(OC_6H_4\text{-}Bu^t)_5(OC_6H_4CH_2CN{\cdot}Ti(Cp)_2Cl]PF_6$ (**5**)

Reaction of $N_3P_3(OC_6H_4\text{-}Bu^t)_5(OC_6H_4CH_2CN)$ with Cp_2TiCl_2 yielded $[N_3P_3(OC_6H_4CH_2CN{\cdot}Ti(Cp)_2Cl)_6][PF_6]_6$ as an orange solid. Coordination of the organometallic fragment with the cyanide-ligand was evident from the increase in the frequency of the ν(CN) band from 2245 cm^{-1} in the free ligand to 2252 cm^{-1}, a behavior typical of the coordination of nitriles with organometallic complexes [27-31]. Thus the expected $\nu(PF_6)$ band was observed at -144.12 ppm.

In the ^{31}P-NMR spectrum, the signal normally observed at 9.1 ppm was shifted with respect to that of the free ligand, to 11.88 ppm, clearly indicating the coordination of the ligand. The ^{1}H-NMR spectrum shows a signal at 6.66 ppm assigned to the proton of the C_5H_5 group of $Ti(Cp)_2Cl$ coordinated to nitrile. Other ^{1}H and ^{13}C signals of the $OC_6H_4CH_2CN$ group were observed normally (see Experimental section), in agreement with those observed for model (**2**). It is interesting to note that notwithstanding the great amount of organometallic derivatives of cyclotriphosphazenes [27-36], those with Ti are scarce. The only reported derivative is $N_3P_3(CH_3)_6{\cdot}TiCl_4$, which was poorly characterized [36]. Thus, the derivates (**3**), (**4**) and (**5**) reported here, constitute the first containing an organometallic fragment coordinated through the titanium atom to the cyclophosphazene ring. Trimer phosphazene compounds (**6**), (**7**) and (**8**) were prepared as reported previously [17, 22] and will not be discussed here.

3.5 Pyrolysis of Organometallic Derivatives of Cycloorgano-triphosphazenes

It is now well known that the thermal degradation of cyclotriphosphazenes often produces cyclolinear and cyclomatrix materials [32, 38-41]. In these cases the cross-linking of the polymeric chains of the cyclophosphazenes produces a high char yield. For the pyrolysis of the organometallic derivatives of the cyclotriphosphazene, a similar mechanism to that of the analogous organometallic derivatives of polyphosphazenes could operate [12-14]. The high pyrolytic yields of these systems were attributed to their extensive coordination cross-linking upon heating. Relatively few thermal studies of organometallic derivatives of cyclotriphosphazene have been reported [32, 33, 38-41]. It is possible that during heating, the organometallic fragments produce vacant coordination sites (especially metal carbonyls [42-44] that are able to coordinate several cyclophosphazenes rings, and in turn each of these rings coordinates with other

organometallic fragments as soon as they are formed, resulting in the formation of a cyclomatrix with the organometallic fragment bonded to the cyclophosphazenes (Scheme 3).

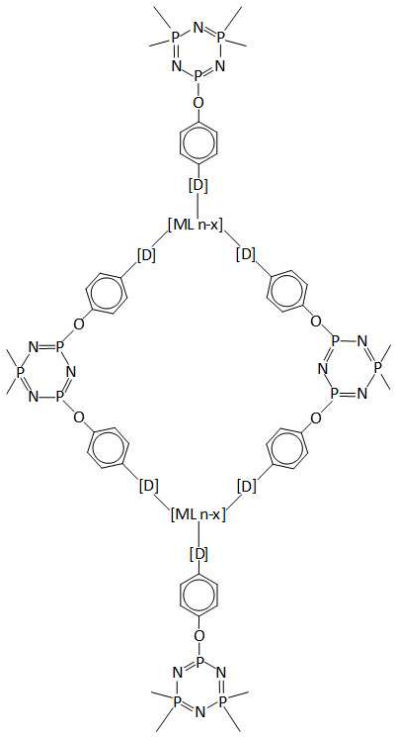

Scheme 3. Schematic representation of the cyclomatrix formed in the pyrolysis of organometallic derivatives of phosphazene trimer.

Pyrolysis of the organometallic derivatives of the cyclophosphazenes (**3**)-(**8**) yields nanostructured metallic materials with composition and morphologies that depend on the nature of the metal, the donor spacer, and on the ratio between the number of organometallic fragments and the number of phosphazene ring units.

From the pyrolysis of the titanium containing cyclophosphazenes (**3**)**,** (**4**) and (**5**), mixtures of the nanostructured materials TiO_2 [45-48] and TiP_2O_7 [49-57] were obtained. The proportion of these phases depends on the proportion of the titanium fragments around the phosphazene ring. For instance, the pyrolysis product from (**3**), which contains a low metal content, yields mainly nanostructured TiP_2O_7, while pyrolysis of the titanium rich cyclophosphazene (**4**) gives a mixture of TiO_2 and TiP_2O_7. Figures 1 and 2 show the TEM, SEM, EDAX and X- ray diffraction patterns of the pyrolytic residues from (**3**) and (**4**), respectively. As shown in the respective SEM

images, the morphology of the products from (**3**) is dense, while that of (**4**) is mostly porous.

On the other hand, the morphology of the pyrolytic products also depends mainly on the nature of the donor spacer. For instance, the pyrolytic product from (**4**) and (**5**), which have the same spacer ($OC_6H_4CH_2CN$), exhibit a porous morphology, although the residue from (**5**) is mostly a three-dimensional monolithic network (see Figure 3b). In contrast, the pyrolytic residue from (**3**) with an oxypyridine spacer, exhibits a dense granular morphology. The morphology of the products is therefore highly sensitive to the nature of the spacer for a specific metal. The XRD patterns exhibited the typical peaks corresponding to TiP_2O_7 and/or TiO_2, in all cases.

From the TEM image of product (**4**) (Fig. 2e), nanoparticles with dimensions of ~20 nm can be estimated. The nanodiffraction image of the products, shown in the inset of Figs (**3**) and (**5**), respectively, indicate a transition from crystalline to amorphous material. EDAX analyses of the pyrolysis products (**3**), (**4**) and (**5**) confirm the presence of titanium and phosphorus, and good agreement with the expected relative amounts of TiO_2/TiP_2O_7, i.e. the Ti/P contents

Nano-sized titanium dioxide particles have been the subject of a great deal of research because of the unique physicochemical properties and applications in the areas of pigments, catalysis and supports, fine ceramics, ion matrices, gas sensors, inorganic membranes, environmental purification and dielectric materials [45-48].

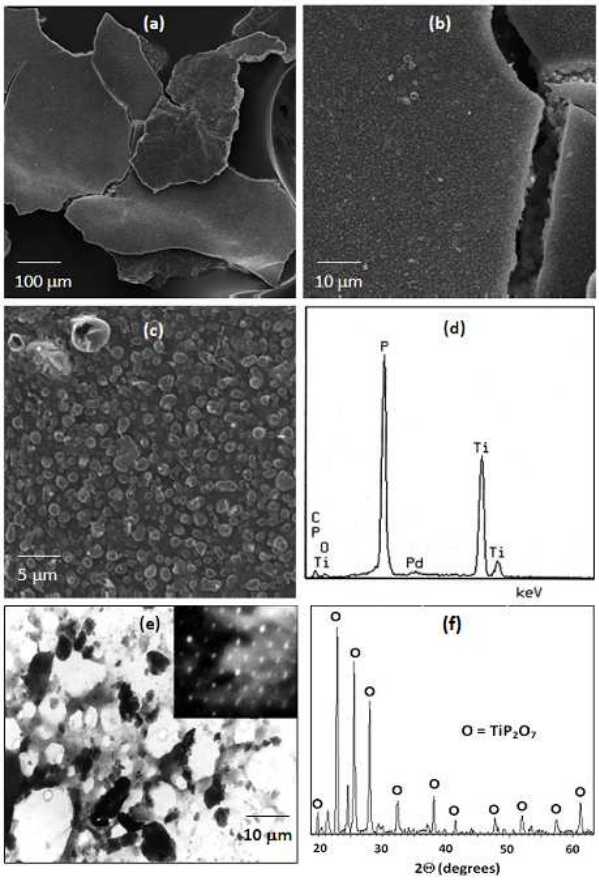

Fig. 1 (a-c) SEM images at several magnifications (d) EDAX (e) TEM image and (f) XRD pattern, of the pyrolysis product from precursor (**3**).

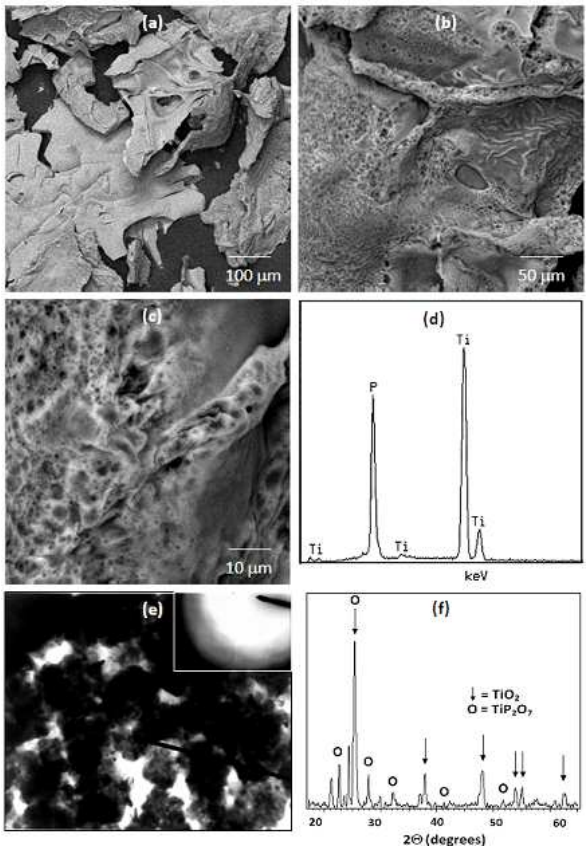

Fig. 2 (a-c) SEM at several magnifications (d) EDAX (e) TEM image and (f) XRD pattern, of the pyrolysis product from precursor (**4**).

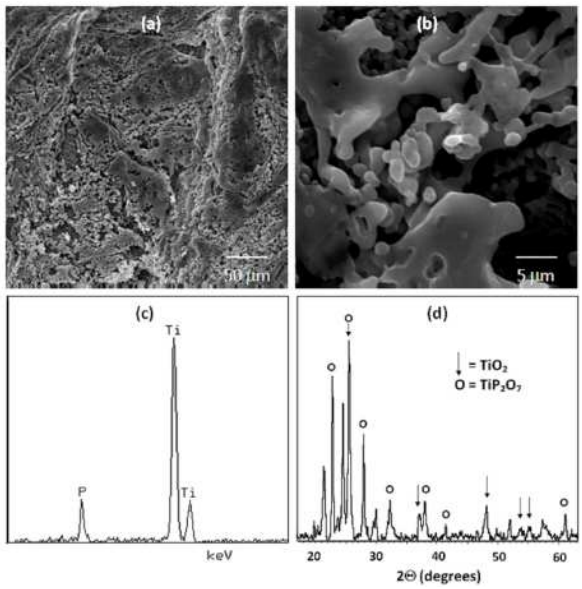

Fig. 3 (a,b) SEM at several magnifications (c) EDAX and (d) XRD pattern, of the pyrolysis product from precursor (**5**).

In the biomaterials field, the use of Ti ceramics as hard tissue replacement implants involves an interaction with the pyrophosphate anion present in bones [49-54].

Although their synthesis [49], structural, spectroscopic [55] and 2D-NMR [56] properties have been studied, to the best of our knowledge no nanoparticles of TiP_2O_7 have yet been reported.

A noticeable effect of the metal on the nature of the pyrolytic residue was seen when the Ru-containing cyclophosphazene, compound (**6**), was pyrolysed. In this case only nanostructured RuO_2 was obtained. Figure 4 shows the SEM, the XRD patterns and the EDAX of this product. Full details of the synthesis of precursor (**6**) [17] as well as their pyrolytic product have been recently reported [58]. The XRD data clearly confirms the presence of tetragonal RuO_2 [59]. The EDAX analysis confirms the presence of only ruthenium, phosphorus and a small amount of oxygen. Main diffraction peaks were seen at 2θ = 28.08, 35.18 and 54.8 (Fig. 4c) and agree well with those reported for RuO_2 [60-62]. The average particle size was estimated to be 11 nm from the Debye- Scherrer relation [58]. The phosphorus atom can arise from the presence of P_4O_7 which itself acts as a solid-state stabilizer [22, 23].

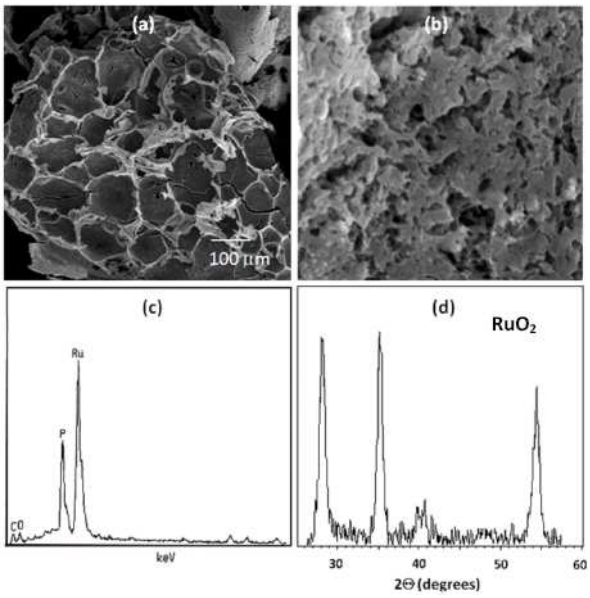

Fig. 4 (a-c) SEM at several magnifications (d) EDAX, of the pyrolysis product from precursor (**6**).

From the pyrolysis of the iron-containing cyclophosphazene, compound (**7**), the product $Fe_2Fe_5(P_2O_7)_4$ was obtained, similar to that obtained in the pyrolysis of the polyphosphazene containing the same iron organometallic fragment anchored to a polymeric chain. Full details of the synthesis of precursor (**7**) have been recently reported [63]. The morphology of the pyrolysis product is porous, as shown in Fig. 5,

and is noted to be similar to the polymer containing the $OC_6H_4CH_2CN$ spacers. EDAX displayed peaks from P and Fe, consistent with the formation of $Fe_2Fe_5(P_2O_7)_4$ as the product.

Finally, the pyrolysis of the tungsten containing cyclophosphazene (**8**) yields a complex mixture of products which were identified by XRD analysis (see Supporting Information, Fig. S1). Among others, WO_3, $P_4O_{7.9}$ and the oxidized 12-tungstate phase with Keggin structure [64-66] were found. It is well known that the preparation of nanostructured WO_3 is usually joined with the oxidized 12-tungstate phase with Keggin structure [64-66].

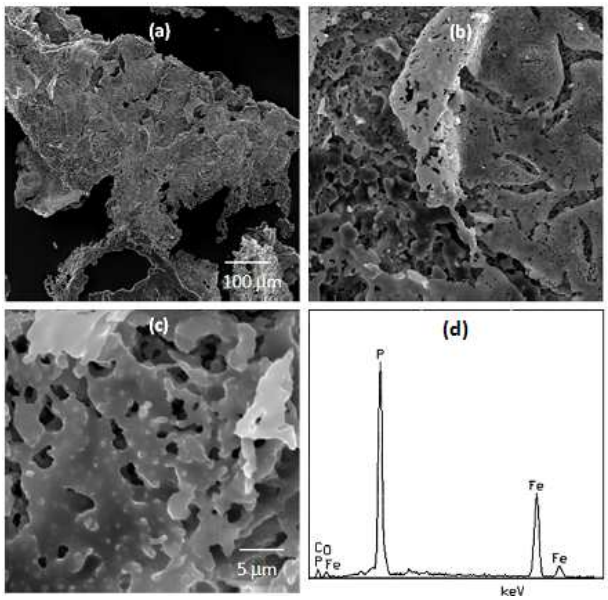

Fig. 5 (a,b) SEM at several magnifications (c) EDAX and (d) XRD pattern, of the pyrolysis product from precursor (**7**).

EDAX analysis, TEM and nanodiffraction image of the pyrolytic product containing W from trimer (**8**) are shown in Fig. 6. The morphology of the material exhibits a dense ceramic-like structure. EDAX analysis shows the presence of W and P. The TEM image (Fig. 6e) shows nanostructures of various size and shape, some of them on the order of ~10 nm in size.

The electron nanodiffraction image shown in the inset of Fig. 6e indicates a somewhat amorphous material. Thus similar pyrolytic products were obtained from polyphosphazene containing anchored tungsten pentacarbonyl fragments [22].

WO_3 is of great interest because of its electrochromic [67], gas sensing [68, 69], and catalytic [70] properties, many of which depend on morphological characteristics such

as particle size, shape and structure. Thus, a considerable effort has been devoted to the synthesis of nanostructured WO_3. The majority of the preparation methods involve the direct reaction of metallic W with oxygen in a variety of experimental conditions [71-74] or evaporation/ deposition of WO_3 [75]. These techniques require complex sample pretreatment and preparation conditions. Few direct and simple chemical methods for obtaining nanostructured WO_3 have been reported due to a lack of simple preparation methods for such materials. Among others, nanostructured WO_3 has been prepared from thermal decomposition of $W(CO)_6$ [75]. The method reported here for preparing WO_3 nanoparticles, although mixed with other phases, constitutes a facile and quick route to obtaining such nanostructured materials.

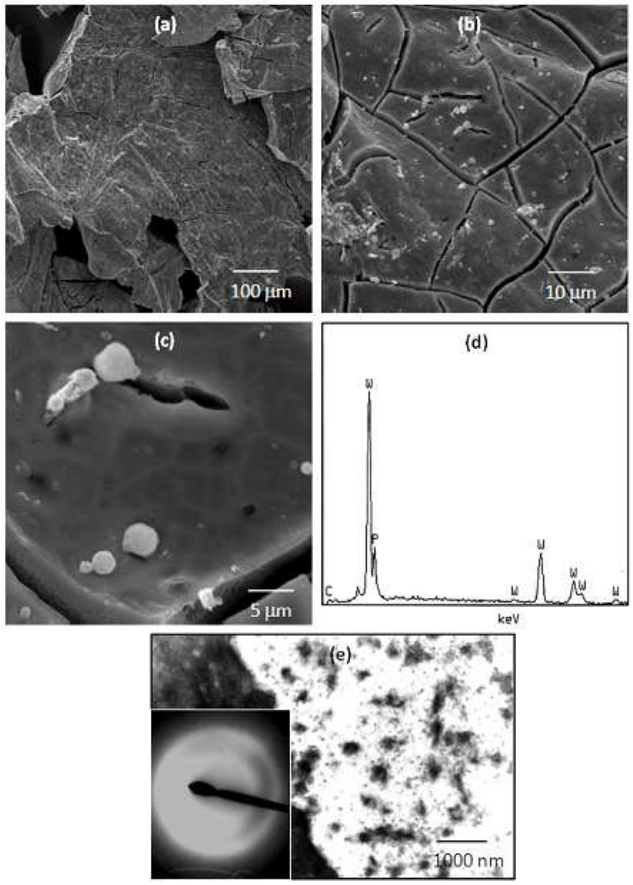

Fig. 6 (a-c) SEM at several magnifications (d) EDAX and (e) TEM, of the pyrolysis product from precursor (**8**).

3.6 Mechanism of Formation of Metallic Nanostructures from Organometallic Cyclic Phosphazenes

Some insight into the mechanism of formation of the metallic nanostructures from pyrolysis in air of the organometallic cyclic phosphazenes can be obtained from the TGA curves (in air) of the cyclic phosphazenes (**3**) and (**4**), shown in Figure 7.

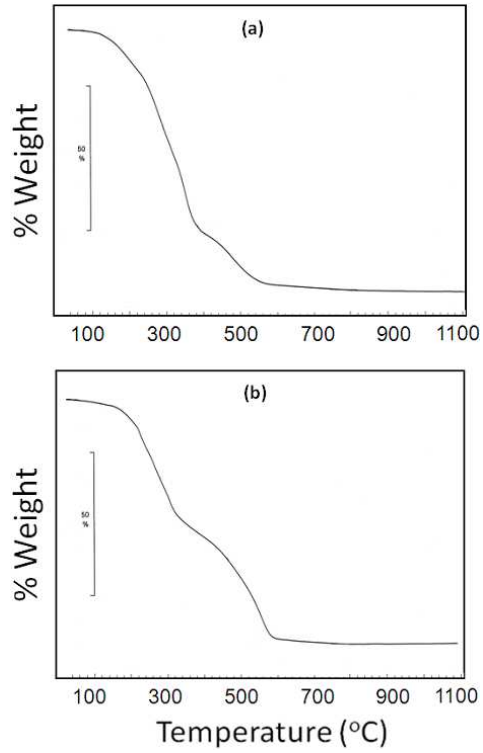

Fig. 7 TGA curve in air of the cyclic phosphazenes (a) (**3**) and (b) (**4**).

For cyclic phosphazene (**3**), the initial small weight loss of 33.6% (calculated 33.19%) can be attributed to a loss of fluorine, chlorine and phosphorus, probably as the respective oxides, in addition to the carbonization of the pyridine group. The second weight loss is assigned to the carbonization of the OC_6H_5 groups, Exp. 30.53%, Calcd. 31.23%. The final weight loss is attributed to the loss of CO_2 from the carbonization of the Cp groups, Exp. 20.78%, Calcd. 21.49%. The final 14.99% of the residue was mainly consistent with the formation of TiP_2O_7 with some small amount of P_4O_7 that is almost always present in the final residues, probably as a stabilizer of the metallic nanoparticles [22-25]. Consistent with this, their DSC curves showed two intense exothermic peaks at 365°C and 483°C in the same zone where the oxidation of the organic matter occurs (see Supporting Information, Fig. S_4,S_7). In agreement with this, their TGA in N_2 is different from that in air (see Supporting Information, Fig. S_2,S_5).

Although several TGA curves in N_2 for organometallic derivatives of polyphosphazenes have been discussed [12-18], similar studies of organometallic derivatives of cylic trimer phosphazenes are scarce. The TGA curve of (**3**) in N_2 shows a gradual weight loss of 4% to 10% between 20°C and 120°C due to the loss of solvent molecules and volatiles generated during the condensation reactions. Above 120°C a sharp weight loss of 75% occurred that is attributed to the total degradation of the material, losing volatile phosphorus compounds similar to those found in the thermal degradation of cyclic trimer without metal [22]. The 12% residue can be explained by the formation of cyclomatrix structures containing metal/organometallic fragments linking several trimer units, similar to the model described in Scheme 3. In addition, the DSC curve, also in N_2 (see Supporting Information, Fig. S_3), displays three strong endothermic events at 350°C, 340°C and 270°C as well as another less intense endothermic peak at 91°C. The latter low intensity peak is assigned to the evaporation of the solvent residues, and the three more intense peaks to evaporation of volatiles molecules generated during the decomposition process. The exothermic peak at 198°C, however, can be attributed to the decomposition processes occurring at around 280°C, a second at 487°C is most likely due to decomposition of some metallic

Similar TGA curves, both in air and in N_2, were seen for the cyclic organometallic titanium phosphazene (**4**), also with similar DSC (Fig. 7b).

Thus, the formation in air of the metallic nanostructure from the organometallic cyclic phosphazenes can be summarized in the following steps:

i) loss or decomposition of some ligands of the organometallic fragment to produce vacant sites, producing a cyclomatrix network;
ii) calcination of the organic matter, which produces holes in the cyclomatrix network, causing the agglomeration of the metallic particles;
iii) oxidation of the phosphorus chain to form phosphorus oxides which bond to the metals to give metal phosphates and/or phosphorus oxides acting as a solid-state matrix, stabilizing the metallic nanoparticles.

3.7 Surface Morphological Studies

Adequate samples for AFM measurements were achieved by depositing a CH_2Cl solution of the precursor over a silicon or SiO_2 surface and dried at room temperature. Subsequent pyrolysis at 800°C in air was conducted to graft the product to the surface. As is shown in Fig. 8a, the morphology of the pyrolytic product from (**3**) exhibits irregular small islands with reasonably uniform dispersion. More detailed features are resolved at higher resolution where in Fig. 8b, quasi-striated structures are observed routinely on top of the rough surface shown in Fig. 8a. The deposited islands for pyrolysis of (**3**) have a mean height of ~20 nm.

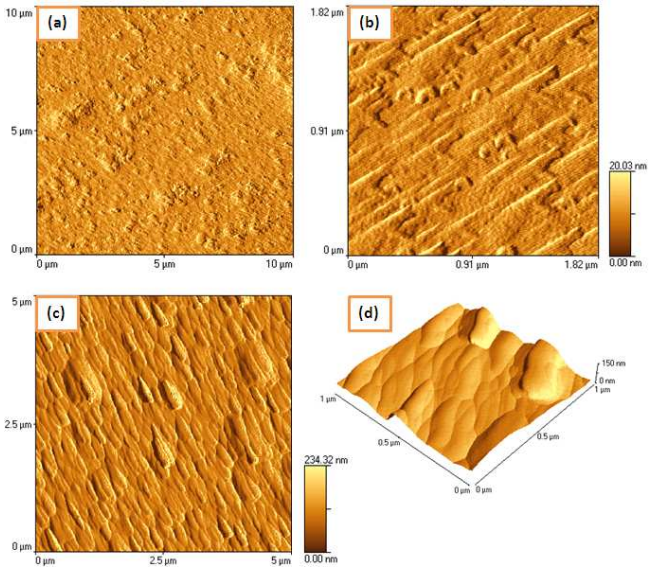

Fig. 8 AFM images of (a,b) the deposited pyrolytic products from (**3**) on silicon surface and (c,d) the deposited pyrolytic products from (**4**) on silicon surface.

Similarly, the morphology of the pyrolytic product from (**4**) on silicon surface shows enlarged high aspect ratio structures with an average height of 64.5 nm, without voids. Higher magnification images exhibit detailed features, dominated by the presence of two height-level structures/islands: one with average height of 67 nm and other of ~140 nm, but of identical phase.

Some of the advantages of this method in preparing metallic nanostructures in the solid-state are the following:

i) the synthetic simplicity in the preparation of the precursor (compared with analogous polymers for instance);

ii) the inorganic metal atom can be distributed uniformly at the molecular level by the formation of a cyclomatrix network;
iii) The holes, or voids formed by the segregation of the organic moieties upon pyrolysis, act as templates for the growth of the nanoparticles. Thus, by choosing different organic spacers in the polymeric chain, the size of the holes may be modulated and the size of the nanoparticles can be controlled.
iv) The diversity of the chemical composition of the organometallic fragments (diverse metals, auxiliary ligands, electron density, etc.) should make it possible to obtain nanostructured materials with predetermined properties, useful for catalysis (Ru, Pt and Au organometallic fragments), magnetics (Fe, Co organometallic fragments), and energy storage/intercalation (Ti organometallic fragments), etc.
v) magnetics (Fe, Co organometallic fragments), and energy storage/intercalation (Ti organometallic fragments), etc.

The possibility of obtaining solid-state metallic nanoparticles by such a synthetic route could potentially allow their application in solid-state sensor materials, catalysis, nanoelectronic devices etc., in addition to fundamental studies of metal nanostructure synthesis.

4 Conclusions

In summary, solid-state pyrolysis of organometallic derivatives of cyclotriphosphazene in air at 800°C yields nanostructured metallic materials with particle sizes on the order of 10-20 nm. The organic spacer of the trimers strongly influences the morphology of the pyrolytic products: the pyridine spacer yields dense structures, while the bencylcyanide spacer yields porous materials. The metal/P ratio of the trimer directly influences the nature of the nanostructured material: a high metal/P ratio yields mostly oxide rich materials, while a low metal/P ratio induces the formation of mostly metal phosphate materials. The auxiliary substituents linked to the cyclic phosphorus also influence the morphology of the pyrolytic products: *t*-butyl groups around the phosphazene ring induce a three-dimensional monolithic network more than those with phenyl groups linked to the phosphorus phosphazene ring, i.e. trimers (**3**), (**6**), (**7**) and (**8**). Similar to the organometallic derivatives of polyphosphazenes as precursors

of nanostructured metallic materials, during pyrolysis of trimer precursors (**3**)–(**6**), the phosphazene trimer acts as a solid-state template, with the phosphorus atoms acting as precursors of the stabilizer as well as of the pyrophosphate.

Supporting Information X-Ray diffraction patterns of pyrolysis from precursor (**8**), TGA and DSC of trimer (**3**) in nitrogen, DSC of trimer (**3**) in air, TGA and DSC of trimer (**4**) in nitrogen, and DSC of trimer (**4**) in air.

Acknowledgment The authors acknowledge the financial support of FONDECYT project 1085011.

References

1. A. S. Edelstein, R. C. Cammarata (ed), Nanomaterials: Synthesis Properties and Applications. J. W. Arrowsmith Ltd, Bristol (2000)
2. K. J. Klabunde in Nanoscale Materials in Chemistry, Wiley Interscience, New York (2001)
3. C. N. Rao, A. Muller A and A. K. Cheetham (ed), The Chemistry of Nanomaterials, Synthesis, Properties and Applications. Wiley-VCH, Weinheim, vol. 2, pp. 170-207 (2004)
4. A. Roucoux, J. Schulz, H. Patin, Chem. Rev. 102, 3757 (2002)
5. J. C. Love, L. A. Estroff, J. K. Kriebel, R. G. Nuzzo, G. M. Whitesides, Chem. Rev. 105, 1103 (2005)
6. M. C. Daniel, D. Astruc, Chem. Rev. 104, 293 (2004).
7. R. Petersen, D. Foucher, B. Tang, A. Lough, N. Raju, J. E. Greedan, I. Manners, Chem. Mater. 7, 2045 (1995)
8. T. Shimizu, T. Teranishi, S. Hasegawa, M. J. Miyake, Phys. Chem. B 107, 2719 (2003)
9. T. Teranis, S. Hasegawa, T. Shimizu, M. Miyake, Adv. Mater. 13, 1699, (2001)
10. M. M. Maye, W. Zheng, L. F. Leibowitz, N. Ly N, Ch. J. Zhong, Langmuir 16, 490 (2000)
11. E. R. Leite, N. L. V. Carreño, E. Longo, F. M. Pontes, A. Barison, A. G. Ferreiro, Y. Manitte, J. A. Varela, Chem. Mater. 14, 3722 (2002)
12. C. Díaz , M. L. Valenzuela in Horizons in R. B. Bregg (ed) Polymer Research, Nova Science Publishers, Chapter 6 (2005)
13. C. Díaz, P. Castillo, J. Inorg. Organomet. Polym. 11, 183 (2002)
14. C. Díaz, P. Castillo, G. A. Carriedo, P. Gómez-Elipe, F. J. García Alonso, Macromol. Phys. Chem. 203, 1912 (2002)
15. G. A. Carriedo, F. J. García Alonso, P. Gómez-Elipe, C. Díaz, N. Yutronic, J. Chilean Chem. Soc. 48, 25 (2003)
16. C. Díaz, P. Castillo, Polym. Bull. 50, 123 (2003)
17. C: Díaz, M. L. Valenzuela, M. Barbosa, Mater. Res. Bull. 9, 39 (2004)
18. G. A. Carriedo, F. J. García Alonso, J. L. García Álvarez, C. Díaz and N. Yutronic, Polyhedron 21, 2579 (2002)
19. M. A. Olshavsky, H. R. Allcock, Chem. Mater. 9, 1367 (1997)
20. C. H. Walker, J. St. John, P. Wisian-Neilson, J. Am. Chem. Soc. 123, 3846 (2001)
21. J. Jung, T. Kmecko, Ch. L. Claypool, H. Zhang, P. Wisian-Neilson, Macromolecules 38, 2122 (2005)
22. C. Díaz, M. L. Valenzuela, Macromolecules 39, 103 (2006)
23. C. Díaz, P. Castillo P, M. L. Valenzuela, J. Cluster Sci. 16, 515 (2005)
24. C. Díaz, M. L. Valenzuela, J. Inorg. Organomet. Polymer 16, 123 (2006)
25. C. Díaz, M. L. Valenzuela, S. Ushak, V. Lavayen, C. O'Dwyer, Journal of Nanoscience and Nanotechnology 9, 1825 (2009)
26. C. Díaz, M. L. Valenzuela, D. Bravo, V. Lavayen, C. O'Dwyer, Inorganic Chemistry 47, 11561 (2008)
27. C. Díaz, I. Izquierdo, Polyhedron 18, 1479 (1999)
28. C. Díaz, I. Izquierdo, F. Mendizábal, N. Yutronic, Inorg. Chim. Acta. 294, 20 (1999)
29. G. A. Carriedo, F. J. García Alonso, J. L. García Álvarez, C. Díaz C, N. Yutronic, Polyhedron 21, 2587 (2002)
30. C. Díaz, F. Mendizábal, Bol. Soc. Chil. Quim. 46, 293 (2001)
31. C. Díaz, M. Barbosa, Z. Godoy, Polyhedron 23, 1027 (2004)
32. M. Gleria and R. De Jaeger (ed) Applicative Aspects of Cyclophospahezenes, Nova Science Publishers, New York (2004)

33. R. De Jaeger, M. Gleria, Prog. Polym. Sci. 23, 173 (1998)
34. V. Chandrasekhar, K. R. Justin Thomas, J. Appl. Organomet. Chem. 1, 7 (1993)
35. V. Chandrasekhar, S. Nagendran S, Chem. Soc. Rev. 3, 193 (2001)
36. M. F. Lappert, K. Srivastaca, J. Chem. Soc. A 193 (1996)
37. H. R. Allcock, Acc. Chem. Res. 12, 352 (1979)
38. D. E. Brown, K. Ramachandra, K. R. Carter, C. W. Allen, Macromolecules 34, 2870 (2001)
39. S. J. Maynard, T. R. Sharp, J. F. Haw, Macromolecules 24, 2794 (1991)
40. D. Kumar, A. D. Gupta, Macromolecules 28, 6323 (1995)
41. H. R. Allcock, G. S. McDonnell, G. H. Riding, I. Manners, Chem. Mater. 2, 425 (1990)
42. G. A. Carriedo, J. F. García Alonso, C. Díaz, M. L. Valenzuela, Polyhedron 25, 105 (2005)
43. H. R. Allcock, K. D. Lavin, N. M. Tollefson, T. I. Evan, Organometallics 2, 267 (1983)
44. H. R. Allcock, A. A. Dembek, E. H. Klingenberg, Macromolecules 24, 5208 (1991)
45. T. I. Trentler, T. E. Denler, J. F. Bertory, A. Agrawd, V. L. Colvin, J. Am. Chem. Soc. 121, 16313 (1999)
46. G. Zhang, L. Gao, Langmuir 19, 967 (2003)
47. Y. Zhang, J. Li, J. Wang, Chem. Mater. 18, 2917 (2006)
48. S. Perera, N. Zelenski, E. Gillan, Chem. Mater. 18, 2381 (2006)
49. I. C. Mancu, J. M. Millet, J. J. Sandulescu, Serb. Chem .Soc. 70, 791 (2005)
50. I. C. Marcu, J. Sandulescu, J. M. Millet, Appl. Catal. A 227, 309 (2002)
51. A. Laachechi, M. Cochez, E. Levy, P. Gaudon, M. Ferrol, J. M. López-Cuesta, Polym. Adv. Techn. 17, 327 (2006)
52. W. Suchank, M. Yoshimine, J. Mater. Res. 13, 94 (1998)
53. J. Sanz, J. E. Iglesias, J. Soria, E. R. Grilla, M. A. G. Aranda, S. Bruque, Chem. Mater. 9, 996 (1997)
54. P. Looss, A. M. Le Ray, G. Grimandi, G. Daculsi, C. Merle, Biomaterials 22, 2785 (2001)
55. K. E. Lipinska-Kalita, M. B. Kneger, S. Carlson, A. M. Krogh Andersen, Physica B 337, 221 (2003)
56. A. G. Dias, L. M. S. Skakle, I. R. Gibson, M. A. Lopez, J. D. Santos, J. Non-Cryst. Sol. 351, 810 (2005)
57. V. Karthuis, N. Khosrovani, A. W. Sleight, N. Roberts, R. Dupree, W. W. Warren Jr, Chem. Mater. 7, 412 (1995)
58. C. Diaz, M. L. Valenzuela, E. Spodine, Y. Moreno, O. Peña, J. Clust. Sci. 8, 31 (2007)
59. F. A. Cotton, J. T. Mague, Inorg. Chem. 5, 317 (1966)
60. M. T. Colomer, J. R. Jurado, Chem. Mater. 12, 923 (2000)
61. L. Ji, J. Lin, H. C. Zeng, Chem. Mater. 13, 2403 (2001)
62. W. Dmowski, T, Egani, K. E. Swider-Lyons, C. T. Love, D. R. Rolison, J. Phys. Chem. B 103, 12677 (2002)
63. C. Díaz C, M. L. Valenzuela, N. Yutronic, J. Inorg. Organomet. Poly. Mat. 17, 577 (2007)
64. N. Xu, M. Sun, W. Cao, N. Yao, E. G. Wang, Appl. Surf. Sci. 157, 84 (2000)
65. M. Sun, N. Xu, W. Cao, E. Wang, J. Mater. Res. 15, 927 (2000)
66. J. F. Keggin, R. Proc, Soc. Ser. A 144, 75 (1934)
67. A. Talledo, C. G. Granqvist, J. Appl. Phys. 77, 4655 (1995)
68. J. Livage, Chem. Mater. 3, 758 (1991)
69. J. L. Solis, S. Saukko, L. Kish, C. G. Granquist, V. Lantto, Thin Solid Films 391, 255 (2001)
70. P. Ponzi, C. Duschatzky, A. Carrascull, E. Ponzi, Appl. Catal. A 169, 373 (1998)
71. G. Gu, B. Zheng, W. Q. Han, S. Roth, J. Liu, Nano Lett. 2, 849 (2002)
72. Q. Han, C. Wang, J. Liu, Adv. Mater. 15, 411 (2003)
73. H. Wang, X. Quan, Y. Zhang and S. Chen, Nanotehnology 19, 065704 (2008)
74. J. Yu, H. Yu, M. L. Guo, S. Mann, Small 4, 87 (2008)
75. K. Hong, M. Xie, R. Hu, H. Wu, Nanotechnology 19, 085604 (2008)